Ion Association and Electrolyte Structure at Surface Films in Lithium-ion Batteries

Justin R. Pinca, William G. Duborg, Ryan Jorn*

Department of Chemistry, Villanova University, Villanova, Pennsylvania 19085, United States

Abstract: During lithium-ion battery charging and discharging, carbonate electrolytes degrade from redox side reactions to produce electrode surface films. The composition of these films depends on the composition of the electrolyte layer at the electrode surface and the structure of the ion solvation shells found therein. However, both the composition and structure of an electrolyte at an interface can vary significantly from their counterparts in the bulk, as reported previously at air and mineral surfaces. Hence, a circular relationship holds in which the surface films formed depend on electrolyte structure which in turn is impacted by the presence of the surface film. In this work three impacts from solid interfaces on carbonate electrolytes are considered: ion accumulation, ion pairing, and solvent exchange dynamics. By considering these effects at four different surfaces of varying solvent affinity (LiF, Li₂CO₃, Li₂EDC, and graphite), we explore the impact of solvent–surface interactions and ion–surface interactions on these interfacial behaviors. Classical molecular dynamics provides a route to explore molecular structure at the electrolyte boundary and two different electrolytes are considered to investigate the role of ion association on accumulation, pairing, and dynamics. By considering the changes as a result of switching between one electrolyte with mostly solvent-separated ions to another with contact ion pairs, we provide evidence that both bulk ion association and the solvent-surface interaction are key descriptors of ion aggregation at the electrode surface. The insights from these simulations not only inform about

^{*} Author to whom correspondence should be addressed: ryan.jorn@villanova.edu

the impacts of battery interfaces on the surrounding electrolyte, but also on the origins of differences reported between classical molecular dynamics simulations at these interfaces.

I. Introduction:

While rechargeable batteries are revolutionizing the way we consume energy, 1-3 challenges remain to advancing the electrolytes at their center. The large number of electrolyte mixtures and materials investigated evidences the challenge in balancing their conductivity between the electrodes with their electrochemical stability at the electrode surface. Nonaqueous liquid electrolytes, in particular, have dominated the advancement of the lithium-ion chemistry that has successfully powered personal electronics and reimagined car engines. Consistent focus has been placed on optimizing the material properties of the electrolytes (e.g. salt solubility, viscosity, ionic conductivity) comprised of linear and cyclic carbonates mixed with lithium salts. However, the importance of the surface chemistry between the electrolyte and the electrodes has complicated the search for new materials, particularly for high voltage applications.

During charge cycling, the electrolyte can undergo direct oxidation/reduction to produce organic polymer compounds and inorganic salts that deposit on the electrode surfaces.^{5,13} Ideally, these films protect the interface from further degradation by blocking additional electron transfers, but allow for continued ion transport. As a result of the desired ion conductivity, the solid film is referred to as a solid electrolyte interphase (SEI). The occurrence of a readily formed SEI at the anode/electrolyte boundary has raised the possibility of tailoring the surface film through modification of the electrolyte composition.^{14–16} In spite decades of research, a clear connection between the electrolyte composition, charge transfer properties at the SEI, and device rate performance remains elusive.^{17,18} The inability to establish structure-function relationships for the

SEI derives, in part, from uncertainty surrounding the structure and dynamics of the electrolyte at this complex interface. ^{19,20} The work presented in this manuscript is focused on the question of how the presence of the SEI changes the electrolyte structure and dynamics, with implications for the evolution of the SEI and device performance.

In order to place non-aqueous battery electrolytes in the greater context of the literature on electrolytes at interfaces, this discussion will be connected with three behaviors reported at aqueous electrolyte interfaces: ion accumulation, ion pairing, and changes in electrolyte dynamics. The behavior of solutions comprised of salts dissolved in water has been explored extensively by both computational modeling and experimental measurements at air/water, ^{21–27} mineral/water, ^{28–} ³³ and liquid/water interfaces. ^{34,35} While the origins and magnitudes of the effects of the interface are still in dispute, three impacts are particularly relevant to the work discussed subsequently. First, there is growing consensus that the boundary can impact the local ion concentration at water interfaces.^{36,37} This effect, termed the specific ion effect, has been shown to favor the migration of larger polarizable anions to the air/water interface and the repulsion of smaller charge dense cations.³⁸ At salt surfaces, similar to those found in a battery at SEI films, the accumulation of positive charges is favored over the anions by the competition between water and anion coordination to the surface-embedded cations. The second impact of note at the electrolyte boundary is an increase in ion association, or ion pairing. ^{29,39–41} The magnitude of the increase in ion pairing between cations and anions at the surface is likely dependent on a complex balance of their attraction to each other, solvation free energies, and the binding of all three components (cation, anion, and solvent) to a second condensed phase. 42,43 In the case of alumina, for example, fluoride was shown to associate more readily with sodium at the mineral surface while other halides did not exhibit greater ion pairing.³³ The third impact of interfaces observed from aqueous

electrolytes is their influence on the local electrolyte dynamics. Ion pairs can cooperatively slow down water rotation⁴⁴ and diffusion in the bulk,⁴⁵ and mineral surfaces can slow local vibrational dynamics.²⁶

While a wealth of literature exists on the behavior of aqueous electrolytes at interfaces, relatively few reports are available for carbonate electrolytes found in lithium-ion batteries. We have previously quantified the behavior of carbonate electrolytes at SEI films in terms of the same three phenomena identified for water mixtures: ion density (accumulation), ion association (ion pairing), and electrolyte dynamics. Our studies were conducted at LiF, Li₂CO₃, and lithium ethylenedicarbonate (Li₂EDC) surfaces, using classical molecular dynamics (CMD), 46,47 since all three compounds have been detected in the SEI formed from ethylene carbonate (EC) mixed with LiPF₆, ¹⁸ We found that lithium ion accumulation was accompanied by increased ion pairing and a slowing of electrolyte dynamics up to a nanometer away from the surface films.⁴⁶ Given previous reports of the dependence of interfacial effects on the simulation model, 45,48-50 comparison of our results with other approaches is vital. The slowing of electrolyte dynamics at the SEI has been corroborated by a recent ab initio molecular dynamics (AIMD) study of EC-based electrolytes at the LiF surface.⁵¹ Ion accumulation has been reported from classical simulations employing explicit polarization at amorphous dicarbonate interfaces, however greater ion association at the Li₂EDC surface was not observed.⁵² We note that comparison with our results in this case is not completely straightforward since the model employed a different nonbonding interaction, a slightly different electrolyte composition, and a significant difference in ion-pairing in the bulk solution far from the interface. In addition to SEI surfaces, CMD simulations have also explored ion adsorption at clean graphite, 53,54 LiFePO4,55 and gold electrode surfaces.56 In the case of graphite, the strength of the lithium solvation shell prevented significant ion accumulation until

the application of voltages approaching the intercalation threshold. In contrast to graphite, significant ion adsorption wells were found at the lithiated iron phosphate surface. With regard to ion association, significant changes in ion solvation structure were seen at gold electrodes for lithium ions dissolved in dimethyl carbonate. These final studies suggest that the impacts of interfaces on battery electrolyte structure and dynamics extends beyond the inorganic films previously considered.

With concerns about the sensitivity of interfacial effects to the inclusion of polarization, it is important to consider the influence of the force field employed on the three impacts previously reported. One of the most straightforward alterations that can be made is reconsideration of the partial charges associated with the atom types. The technique of charge scaling has been discussed extensively for applications to bulk water solutions and has been shown to improve the solvation structure and diffusion properties of simple ions in comparison to their unscaled counterparts.⁵⁷ The use of scaled charges has found a rigorous explanation as a means of including the mean field polarization of the solvent. 58,59 While normally suspect for applications at interfaces of discontinuous dielectric constant, some success has been demonstrated at surfaces when the change in dielectric is less abrupt than the water/air interface.³⁴ Chaudhari et al. applied the technique to develop a solvent charge-scaled model for ethylene carbonate (EC) and greatly improved its coordination with lithium as compared to AIMD.⁶⁰ By scaling the atomic partial charges, the EC dipole was corrected to match the value from condensed phase environments with greater fidelity than charges taken from gas phase calculations with electrostatic potential fitting (ESP).⁶¹ In this report, we seek to expand our previous investigation to consider the impact of ion association, tuned by the use of charge scaling, on ion accumulation, ion pairing, and electrolyte dynamics. While not intended as a replacement for the accuracy of explicit polarization, 62 this

approach allows us to compare the behavior of two electrolytes: one that produces solvent-separated ion pairs in the bulk environment, with a solution that contains more tightly coordinated contact ion pairs in bulk. This work contributes to understanding the general role of ion association and surface-solvent interactions on the electrolyte structure and dynamics at SEI interfaces. By making use of a variety of CMD simulations, we show how weakened solvent interactions result in substantial changes to the ion accumulation, association, and dynamics that provide some insight into the differences reported for simulations of electrolytes at the SEI interface.

II. Methods:

The SEI/electrolyte interface was described throughout using a previously developed Class 2 force field (CFF), 46,53 and the interested reader is referred to the cited works for more details. The CFF model has been shown to accurately describe the structure and thermodynamics of carbonates⁶³⁻⁶⁶ and the bonding terms in our classical molecular dynamics (CMD) simulations were taken directly from the CFF91 parameter file included with the LAMMPS distribution.^{67,68} The partial charges for EC, LiPF₆, Li₂EDC, and Li₂CO₃ were chosen to reproduce electrostatic potentials (ESPs) from gas phase calculations within density functional theory (DFT) using the PBE functional and a 6-311G** basis set. 46,53 The ESP fitting was done within CP2K⁶⁹⁻⁷¹ and all CMD simulations were carried out within LAMMPS. The original partial charges were incorporated in the "non-scaled" model discussed extensively throughout the remainder of this manuscript. A charge-scaling approach was adopted in order to study the interplay of ion association and solvent-surface interaction with electrolyte behavior at the SEI. Chaudhari et al. showed that the use of scaled charges on EC relaxed the exaggerated solvation structure of the lithium ions in the bulk phase that often occurs when relying on two-body nonbonded forces. 60,72 Following the work of Chaudhari et al., a second model was developed by multiplying the charges

on EC by a factor of 0.9 to account for mean field polarization in the bulk electrolyte. This second model will be referred to as the "q-scaled" model in the discussion that follows and provides a contrast of greater ion association relative to the non-scaled model. As shown subsequently, scaling the charges on EC caused a transition from solvent-separated ion solvation structures in the CMD simulations to contact ion pairs between the salt ions. Hence, the q-scaled model served as a means to study general electrolyte behavior at various interfaces. Contrary to the observations from Chaudhari et al., we found that attempting to scale the charges on EC more aggressively, multiplying by 0.8 rather than 0.9, led to unphysically large aggregation of the lithium salt at the temperatures considered and was not explored further. It should be kept in mind that though the model bears the title "q-scaled", only the EC charges have been scaled and none of the other species had their partial charges altered from the DFT results. The long-range electrostatic interactions were included in the simulations via the PPPM approach and a 9-6 Lennard-Jones potential was used to account for the remaining nonbonded interactions. The Lennard-Jones parameters were chosen based on CFF91 atom types and mixing rules, with the exception of the EC and LiPF₆ interactions which were previously force-matched to AIMD trajectories.⁵³

Simulation cells for bulk electrolyte were filled by random packing and models of the SEI/electrolyte interface were constructed by dividing the box into three sections, see Figure 1, for the molecular structures and the box setup. The bulk electrolyte simulations used an initial 50Å x 50Å cube containing 1129 EC molecules and 75 LiPF₆ formula units. For simulations of the SEI interface, electrolyte was added to the center section of the simulation cell at a concentration of 1.2M and a density in agreement with the results from the bulk simulations. The electrolyte region was built with a concentration higher than the usual 1.0M to account for the accumulation of ions at the surfaces. As seen in previous simulations, ions quickly adsorb to the

SEI surfaces, reducing the bulk concentration to around 1.0M in most cases. The two outside sections of the cell were filled with the SEI material and the entire cell was subjected to periodic boundary conditions in all three dimensions. Two different approaches were taken for packing the SEI boxes in accord with recent transmission electron microscopy studies that show both amorphous and crystalline regions in the surface films.^{73–76} Following our previous work, crystals of LiF and lithium carbonate were considered with the [100] face of LiF and the corrugated [010] face of Li₂CO₃ wetted by the electrolyte. In both cases the bulk lattice vectors were used to recreate the crystals from their unit cells in the SEI regions. Since Li₂EDC represents a larger oligomer (for the molecular structure see Figure S1 in the Supporting Information), it was assumed to be amorphous and these SEI regions were packed randomly using Packmol.⁷⁷ The starting width of the electrolyte region in the Z direction (see Figure 1) is 160 Å and the width of the two SEI regions are around 20 Å each, subject to the constraint of fitting the required number of unit cells for the crystalline films. The electrolyte region was made much longer than the SEI boxes to guarantee that the center of the electrolyte region would have bulk-like behavior with minimal surface effects. (See Supporting Information for the number of molecules added in each simulation). The cross sections of the SEI simulation cells in the xy-plane were chosen to be around 70Å x 70Å for the inorganic crystalline films and 60Å x 60Å for the amorphous Li₂EDC. By comparison with smaller box sizes, it was determined that such large cross sections were necessary to provide reasonable convergence of the surface structure over the course of 40ns simulations.

Each simulation cell was equilibrated following construction, beginning with the bulk electrolyte using both the non-scaled and q-scaled force fields. For both bulk simulations, the system was heated from 0K to 453K using a Langevin thermostat followed by 5 ns of simulation at 1 atm via a Nose-Hoover thermostat and barostat. The densities found from these simulations

were used to build the SEI interface cells which were equilibrated by applying the same simulated annealing technique used in a previous study.⁴⁶ For the crystalline SEI films, the lattice configurations were frozen during the simulation and annealing was carried out on the electrolyte to drive faster equilibration of the surface structure. The electrolyte was heated to 1200K using a Langevin thermostat, propagated for 5 ns with a Nose-Hoover thermostat, and then cooled back to 453K and equilibrated for another 5 ns. In the case of the amorphous Li₂EDC film, the SEI films were first annealed under NVT conditions and the SEI portion was heated past its melting point to 900K. Following the heating of the SEI film, it was allowed to evolve for 2 ns and then gradually cooled back down to 453K over 2 ns. Once the SEI was finished annealing, the whole system (SEI+electrolyte) was equilibrated at 1 atm of constant pressure and 453K for 3 ns. For all three types of SEI simulation cells, production trajectories were collected over an additional 40 ns at 453K. As noted in previous work, 46,52 higher temperatures than typical operating conditions (300K) were used to accelerate the simulations and convergence of electrolyte densities. Faster convergence of the calculated ion densities and solvation structures were particularly important for the final set of resource-intensive simulations carried out at graphite electrodes.

Having considered the impact of charge-dense inorganic films, the bare graphite electrode interface provides a contrast with tunable electrolyte–surface interactions. Figure 2 shows the configuration of the electrode interface as a series of graphite sheets in contact with a solution of EC and 1M LiPF₆. At low voltages, ions do not accumulate at graphite as a result of the weaker van der Waals attraction competing against the strong coordination of EC in the lithium solvation shell. However, our interest was also in considering the impact of an applied voltage and previous investigations of the graphite/SEI/electrolyte interface showed the importance of including both electrode polarization and applied voltage.^{53,54} As a result, the image charge method developed by

Petersen et al. was implemented within LAMMPS to treat the graphite electrode as a perfect conductor and to consider two different voltage differences across the electrodes in the simulation: 0V and 3V (a drop of roughly 1.5 V on either side of the simulation cell). ⁷⁸ The same strategy for implementing the electrostatics was used as discussed in Ref. 56. In both instances, the nonperiodic nature of the electrode configuration was accounted for in the PPPM evaluation and a similar size simulation cell was employed (namely 26.77Å x 25.524Å x 105Å). The initial configurations for these electrode simulations were generated by randomly placing 36 LiPF₆ and 511–540 EC molecules in the electrolyte section of the cell followed by addition of the graphite particles and images charges on either side. Interactions with the image charges were included as the electrolyte was heated up to 450K and equilibrated for 5 ns under NVT conditions with a Nose-Hoover thermostat. As in the cases with the SEI simulations, production trajectories were carried out for an additional 40 ns.

III. Results and Discussion:

a. Comparing Non-scaled and Q-scaled Bulk Electrolytes

The changes in the bulk electrolyte structure as a result of swapping the non-scaled and q-scaled force fields demonstrates the relevance of these models to exploring ion association at the interface. Figure 3 contrasts the ion pairing in the bulk phase of the non-scaled and q-scaled solvents and shows that while the shape of the radial distribution functions (RDFs) do not change, the magnitudes of the peaks differ substantially. As expected, the peak in the Li–P RDF occurs between 3–4 Å since the fluorines attached to the phosphorous take part in the first solvation shell and not the phosphorous directly. In the non-scaled electrolyte, the average coordination of the lithium ions by PF₆⁻ is 0.3 phosphorous atoms with 73% of lithium solvation structures not containing any coordinating phosphorous. While Figure 3 refers to the bulk electrolyte at the

elevated temperatures used in subsequent simulations (453K), the results at 313K demonstrate even greater ion dissociation (see Figures S2–S3 in the Supporting Information). The solvent separated nature of the ion pair in the non-scaled solvent is in agreement with preferences found from AIMD simulations,^{79,80} Raman spectroscopy,⁸¹ NMR spectroscopy,^{82,83} and studies of similar cyclic carbonates.^{84–86} However, the degree of ion dissociation is more extreme than that seen in the CMD work of Borodin and Smith who showed much tighter ion pairing with an average coordination number of 0.8 to 1.2 phosphorous atoms in the bulk electrolyte.⁸⁷

The impact of the q-scaled model is to fundamentally alter the ion association by increasing anion coordination. Figure 3 shows that with the q-scaled force field, phosphorous coordination increases to an average of 1.04 atoms with 38.1% of lithium solvation structures having a single phosphorous and 30.0% containing multiple phosphorous atoms. The increase in coordination by PF₆⁻ is matched by a decrease in EC carbonyl oxygen coordination to lithium (see Figures S2–S4 in the Supporting Information), which drops from 4.18 in the non-scaled solvent to 3.37 in the qscaled description at 453K. The difference in ion association seen between the two electrolytes at 453K is also seen in comparison between the q-scaled and non-scaled results at 313K, as shown in the Supporting Information. The RDF between phosphorous and hydrogen from the EC molecules shows a much weaker solvation structure for the anion, consistent with a much weaker anion-solvent interaction (see Figure S5 in the Supporting Information).⁸⁸ Nevertheless the coordination number for hydrogen surrounding the phosphorous anion also drops from 24 to 20 in comparing the non-scaled and q-scaled results. Given the 4 hydrogen atoms per EC molecule, the loss in EC coordination for the anion agrees with the loss of about one EC from the lithium solvation shell.

Having shown how charge scaling tunes the electrolyte from salt dissociated to ion pairing, we next considered changes to the electrolyte dynamics. The diffusion coefficient for Li⁺ with the dissociating salt model (non-scaled) is $1.00 \times 10^{-10} \frac{m^2}{s}$ at 313K, while the result within the ionpairing model (q-scaled) shows a slightly higher result of $1.29 \times 10^{-10} \frac{m^2}{s}$. Both results agree reasonably with reports from NMR studies suggesting the lithium diffusion coefficient as $1.53 \times 10^{-10} \frac{m^2}{s}$, 89 and show the customary increase in ion mobility with charge scaling. The diffusion coefficients for EC and PF₆⁻ at 313K also agree well with experiment (39% and 45% error respectively in the non-scaled electrolyte). In comparing the diffusion of EC and PF₆⁻ in the non-scaled and q-scaled electrolytes, they follow the same trend as Li⁺ of greater mobility with charge scaling with increases of 60% and 22% respectively. Naturally, with increased temperature the Li⁺ diffusion coefficient increases and is found to be $10.66 \times 10^{-10} \frac{m^2}{s}$ at 453K within the non-scaled electrolyte and the EC diffusion coefficient is found to be $21.57 \times 10^{-10} \frac{m^2}{s}$, about an order of magnitude larger than their reported values at 313K,83,89 but within a factor of 2 of values reported at 363K.87 The impact of the q-scaled force field on diffusion at the higher temperature remained minor: the diffusion coefficient for lithium increased by 16% and that of EC increased by nearly twice that amount, 31%. In contrast to the lithium ion and EC solvent, the anion diffusion coefficient decreased by 14% of its original value $(14.81 \times 10^{-10} \frac{m^2}{s})$ at 453K. The decrease in PF₆⁻ diffusion is a direct result of the increase in ion pairing upon charge scaling, as evident from the ratios of the diffusion coefficients. The value of $\frac{D_{PF_6}}{D_{I,i}}$ decreased from 1.4 in the nonscaled electrolyte to 1.0 in the q-scaled simulation at 453K, indicating that the average motion of the anion becomes more closely coupled to that of the cation.

The greater coupling of the ion motion in the q-scaled result was also reflected by changes in the observed solvent residence time, τ_{Li-P} , shown in Figure 4. The residence time is extracted from the solvation residence correlation function defined by:

$$\langle H_{solv}^X(0)H_{solv}^X(t)\rangle \tag{1}$$

where $H_{solv}^X(t)$ is a Heaviside function that gives a value of 1 when species X is within a cut-off distance from the lithium ion, and 0 otherwise. The brackets in Eq. 1 indicate an average across all lithium ions and over different time origins during the production trajectory. Figure 4 shows that the anion remains stuck to the lithium much longer in the q-scaled electrolyte with the residence times lengthening by a factor of five (0.17 vs. 0.92 ns). The factor of five is unique to the phosphorous residence time, however, since the EC lifetime remain relatively unchanged (0.076 vs. 0.087 ns) in the electrolyte with contact ion pairs (q-scaled) versus dissociated salt (non-scaled model) (see Figure S6 in the Supplemental Information). Thus the solvent exchange remains faster than the time scale associated with the anion, in agreement with Borodin and Smith.⁸⁷ In summary, by considering the changes in solvation structure and dynamics, it is clear that the non-scaled electrolyte favors a solvent-separated ion pair in the bulk electrolyte whereas the q-scaled electrolyte results in greater ion pairing and coupled transport. The question we seek to address in the remaining sections is whether this difference in ion association affects previous observations of ion accumulation, pairing, and dynamics at the SEI surfaces.

b. Ion Accumulation at SEI Interfaces

The ability for interfaces to attract ions can alter the chemistry observed at the electrode/electrolyte surface. For example, Lu et al. have proposed using very high concentrations of lithium salt (5M) to form a reversible protective coating for the electrode surface that would

avoid the loss of active lithium to the formation of a long-lived SEI film. 90 Under the application of a bias voltage, the migration of ions to the graphite surface helps to exclude the solvent and provide greater electrochemical stability to the electrode surface. Specific ion effects that increase local anion concentration at the battery interface could play a similarly critical role in determining surface chemistry. Figure 5 shows the resulting density profiles for the three SEI surfaces considered. In each case it is clear that the interface favors local accumulation of salt ions independent of the bulk electrolyte properties, in agreement with prior reports using both simple pairwise nonbonded interactions and many-body explicit polarization. 46,52 Beginning with the LiF surface, it is clear that the degree of ion association does not impact the location or the magnitude of the first maxima in the lithium or hexafluorophosphate densities. Indeed, the lithium density is nearly indistinguishable between the two models and the anion peak is only slightly higher in the q-scaled electrolyte. The first maxima in the ion densities correspond to the adsorbed layer of the ions directly exposed to the LiF surface and shows a very tight peak for the small lithium ions, followed by a broader feature for the larger anions which are less strongly attached to the surface. The identification of the anion peak arising from adsorbed species comes from the observation that the peak occurs roughly 1Å away from the maximum in the lithium density. In the bulk solution, the Li-P RDF shows a separation around 3.2Å, so the anion density increases too closely to the lithium ions to be a second layer attached to the adsorbed lithium layer. This conclusion is supported by the RDF's at the surface which show the growth of a new peak around 2.5 Å from the lithium ion that arises from the surface bound anions. The increase in anion density at the interface is presumably a result of weaker coordination of surface lithium by the q-scaled EC solvent. The correlation between the small change in anion density and EC density at the crystal surface is verified in Figure S7 (see the Supporting Information) by comparing the non-scaled and q-scaled electrolytes. Since all of the density plots in Figure 5 are normalized with respect to their bulk values, it appears that the change in bulk ion association is not as important as the reduction in the EC–surface interaction.

In contrast to LiF, the non-scaled and q-scaled electrolytes differ more significantly at the lithium carbonate surface. Since the [010] surface of lithium carbonate is corrugated, and surface relaxation is ignored for simplicity, there are two peaks in the lithium ion density over the first several angstroms from the surface. The first peak corresponds to lithium ions settling into the valleys present on the surface between alternating layers, while the second represents coordination to the surface oxygens that protrude further into the electrolyte on alternating layers. The first peak in the lithium density is rather unaffected by the change in nature of the solvent, consistent with the facts that these ions must shed most of their bulk solvation structure to occupy the valleys on the surface and that the EC molecules do not compete with the lithium to coordinate these sites. The second lithium peak, however, increases by nearly a factor of two in the ion-paired electrolyte. The increase in lithium density with ion association is a result of two factors: 1) weaker lithium coordination by EC allowing for stronger association with the surface oxygens and 2) greater ion association with the anions which can also adsorb more readily. Not only is more lithium found at the crystal surface, but there is an increase in the amount of anion present in the q-scaled electrolyte. Consulting the density plot for EC with respect to the lithium carbonate surface (see Figure S7) shows that the effect of q-scaling significantly changes the coordination of EC at the crystal film allowing for more anions to adsorb.

The difference in EC behavior at LiF versus lithium carbonate remains connected to the interaction of the EC with the surface groups. In the case of LiF, the EC lay flatter against the crystal and form several contacts with the underlying surface charges, as shown previously.⁴⁶ In

the case of Li₂CO₃, the EC orient more perpendicular to the crystal surface and coordinate either by contact between the crystal lithiums and the EC carbonyl oxygen, or between the surface oxygens and the EC hydrogens. Having less exposure to the surface makes the EC interaction more dependent on the charge on a single atom (the carbonyl oxygen) and thus more sensitive to the scaled charges in competition with the anion. Hence, in the case of lithium carbonate, both the weakened EC–surface interaction and the greater ion association present in the q-scaled electrolyte allows for greater lithium accumulation.

The significant change in ion accumulation with greater bulk association seen for lithium carbonate carries over to the lithium ethylenedicarbonate (Li₂EDC) surface. Given its amorphous structure, the location of the "surface" for this SEI layer was determined from the crossing point of the dicarbonate density and the EC density (See Figure S5 in Supporting Information). The magnitude of the ion accumulations in this case are smaller than the previously discussed crystals, whether referring to the non-scaled or q-scaled electrolytes. The smaller accumulations are presumably due to the disordered nature of the SEI and the more diffuse nature of its charged carbonate groups in comparison to the compact, charge-dense ionic crystal surfaces. Another related difference between the Li₂EDC surface and the previously discussed crystals is the lack of a strongly structured EC layer at the surface.⁴⁶ The density of EC is relatively flat at the Li₂EDC surface (see Figure S7) and only gradually drops to zero by deformations in the surface film at the Angstrom length-scale. The lack of EC ordering and density changes indicate that the EC-surface interaction is not as strong as seen for the previous films. Ion accumulation is therefore more dependent on the weakened ion solvation shell in comparing the q-scaled and non-scaled results. This conclusion is based on the lack of significant changes in EC density with changes in ion association, in contrast to the behavior at the lithium carbonate surface, yet persistence of the

increased ion density. The connection between strength of the solvation shell and ion accumulation comes from the greater ability for Li₂EDC to coordinate electrolyte lithium ions with fully charged carbonate groups. Ion accumulation in this case is driven less by changes to the EC-surface coordination and more so by the changes in bulk ion association. Beyond the noted changes in the ion densities, a second impact of the q-scaling at Li₂EDC is to allow the EC solvent to form slightly deeper protrusions into the SEI material, as shown by the EC density profile in Figure S7 (See Supporting Information), and the deeper ion penetration seen in Figure 5(c).

To summarize the results for the inorganic SEI, all exhibit ion accumulation and in all cases the use of the q-scaled solvent increased the densities of ions present at the interface. The origin of the differences between the non-scaled and q-scaled electrolytes varies dependent on the strength of the EC–surface coordination. When the EC is strongly bound to the surface, the increased ion accumulation arises strictly from changes to the EC-surface interaction, for example the case of strongly bound EC at the LiF surface. However, when the EC is more weakly bound to the surface, accumulation is more sensitive to bulk ion association, as seen in the case of lithium carbonate and Li₂EDC. These findings suggest that not only is it important to recover accurate bulk solvation structures, but to also accurately account for the EC–surface interaction at inorganic crystal film surfaces.

In contrast to the inorganic SEI films, the edge plane of graphite demonstrates ion depletion from the surface layer rather than accumulation. As shown in Figure 6, the normalized ion density in the electrolyte layer at the negatively charged electrode, less than 5Å from the surface, drops below the bulk value for both the 0V and 3V simulations. The exclusion of lithium from the graphite surface is caused by a shift in the balance between ion–surface attraction and the EC solvation shell from the case of the inorganic surface films. In contrast to the SEI surfaces, which

attracted ions based on electrostatic binding to embedded surface charges, the energetic cost for ion desolvation is not compensated at graphite by the gain in surface interactions. For our model of the graphite electrode particle, interactions with ions are limited to a combination of weaker van der Waals forces and image-charge interactions. In contrast to the ions, the EC forms a structured layer at the surface that also discourages ion migration (see Figure S8 in the Supporting Information).⁵³ Within the context of our previous discussion, one can anticipate that with the stronger EC-surface interaction, the impact of this interface on the ion density will be minimal. The favoring of bulk solvation over surface interactions at the graphite surface is also seen in the anion density. Hexafluorophosphate is solvated more weakly by EC, allowing for a larger amount of anion accumulation near the surface and a shifting of the anion density maximum closer to the surface. The depletion of both ions in the first layer at 0V is balanced by accumulation in the second layer of the electrolyte, from 1.6 to 2.0 times their bulk values. With an applied voltage (and concomitant addition of negative surface charge density to the right electrode surface), the amount of lithium seen at the right electrode increases substantially, in excess of 6 times its bulk value, but remains separated from the electrode surface by the first layer of EC.

Turning to the impact of bulk ion association between the two electrolyte models, the same trends are shown as in the case of the inorganic surface, but in the limit of even stronger EC-surface interactions than seen for LiF. The EC density at graphite is unchanged while the ion densities see significant reductions in local accumulation with greater ion pairing. At 0V, the lithium density is reduced by 27% from the peak seen for the non-scaled model and the reduction is more substantial with applied voltage. At 3V the reduction in the lithium ion density between the non-scaled and q-scaled electrolytes is close to 60%. For the simulations at 0V and 3V, the smaller lithium density using the q-scaled solvent must depend on the difference in the bulk solvation structures since

there is minimal direct contact with the surface. The diminished attraction to the right electrode arises from the difference in interaction between the partially screened electrode and the closely coupled ion pairs in the q-scaled solvent versus the dissociated ions, in analogy to the trend seen for ion conductivity with changes in ion association.⁸⁴ In summary, ion accumulation near surfaces (beyond the first adsorbed layer), is more sensitive to the bulk electrolyte behavior than when they strongly adsorb to the surface.

c. Ion Pairing at the Interfaces

A direct correlation has been observed between systematic changes to the lithium ion solvation shell and the composition of the SEI at the electrode surface. The correlation has been investigated in experiments altering co-solvent ratios, 91 salt concentration, 92 and the identity of the anions coordinating to the lithium ion. 93 Hence, the ability for the SEI interface to drive changes in ion solvation structure will likely impact the continued evolution of the surface film. Given that the non-scaled and q-scaled electrolytes differ significantly in their bulk phase ion association, the question that naturally arises is whether these changes in bulk solvation alter the coordination behavior as one approaches the SEI surface. Figures 7–8 show the changes in coordination number as the lithium ion approaches the Li₂CO₃ and Li₂EDC surfaces, respectively. As can be seen in the case of the lithium carbonate, the lithium solvation shell takes on more anions in exchange for the EC coordination as one moves towards the adsorbed layer. Since the bulk value for the anion coordination is 0.3 in the case of the non-scaled solvent, the surface coordination jumps to around 1.9 phosphorous atoms at the film surface. The transition in solvation environments is aligned with the predicted increase in ion density at the surface, but the magnitude is surprising given that it spans the range from solvent-separated in the bulk to an aggregated structure involving multiple coordinated anions at the surface. The change in ion association for the q-scaled electrolyte is less

extreme relative to its bulk value but also predicts a transition to a highly aggregated structure at the crystal surface (from roughly 1.0 atom in bulk to 3.0 coordinating anions at the surface). Both models follow the same relative decline in EC coordination commensurate with the spike in anion coordination. The same effect is seen in the case of LiF (see Figure S9 in the Supporting Information), suggesting that at ionic crystal surfaces the impact of increased bulk ion association is to reduce the relative change in coordination number and to give aggregated structures similar to those seen for solvent-separated ions. This observation provides a possible clue to previous disagreement with the observations of Bedrov and Borodin, 52 since their model possessed greater bulk ion association which could lead to more moderate relative changes at the surface.

Figure 8 serves to provide a puzzling addition to this study since it shows very minimal relative changes in solvation structure at Li₂EDC when switching from the non-scaled electrolyte to the q-scaled solvent. The overall anion coordination numbers at Li₂EDC are smaller than those seen for the inorganic crystals, in agreement with the lesser amount of ion accumulation discussed previously. However, the trend with ion association that was seen for the inorganic crystals is not repeated here. With increasing salt pairing in the bulk solution, one does not see a dramatic difference in coordination at the surface with respect to bulk. In the case of the non-scaled electrolyte, i.e. low salt association, the coordination increases to 0.76 which is still a bit less than a contact ion-pair on average. In the case of the q-scaled electrolyte, i.e. higher salt association, the coordination increases to 1.75 which is nearly the same relative increase as seen for the non-scaled solvent with respect to its bulk value. The anion coordination does remain higher for the q-scaled solvent as one moves into the SEI film region, however this is likely connected to the deeper penetration of the electrolyte into the SEI. The link to electrolyte penetration is supported by the lower Li₂EDC oxygen coordination in the q-scaled simulation.

One explanation for the differences in behavior between the inorganic crystals and the Li₂EDC surface is that the crystals drive such a strong adsorption of lithium at their rigid boundary that the adsorbed electrolyte layer saturates with ions. Hence there is no room to accommodate larger aggregates and the q-scaled electrolyte is limited in how much the anion coordination can increase at the surface, having started with contact ion pairs in the bulk environment. In the case of Li₂EDC, the ion accumulation is less severe which prevents the same type of saturation and permits both the non-scaled and q-scaled results to increase in their coordination by similar amounts in response to their interaction with the amorphous surface and the weakened EC–Li attraction. Regarding the surface interactions in the models used, overestimation of the binding of the ions to the Li₂EDC surface could also produce an artificially high perturbation of the lithium solvation structure at the interface. One obvious omission in these simulations is the exclusion of additional polarization considerations for the SEI molecules themselves which could diminish the coordination of the lithium salts by the dicarbonate group and further shrink the maxima seen in Figure 8.⁴⁹

The connection between surface attraction and changes to solvation structure is further supported by considering ion solvation at the graphite particle, shown in Figure 9. In the study of ion accumulation, we noted that the weak interaction with the graphite surface did not favor ion adsorption. The plots of coordination in the lithium ion solvation shell as it approaches the graphite particle show that the weaker interaction also has minimal impact on the solvation structure around the lithium ions. At 0V, both the non-scaled and q-scaled electrolytes showed relatively flat EC coordination profiles. The non-scaled model showed no change up to 4.5 Å from the surface and the q-scaled result showed only a slight increase (approx. 20%) in EC coordination near the surface. Regarding ion association, both the q-scaled and non-scaled results show little change in

PF₆⁻ coordination up to 7.5 Å from the surface. In the 3 Å layer near the surface there is a drop in anion coordination to ½ of the bulk value in both the non-scaled and q-scaled electrolytes, suggesting a loss of ion association directly at the graphite surface. However, these configurations are not energetically favorable and represent a very small population, as shown by the very low density of lithium ions in this region in Figure 6. With the application of a voltage across the simulation cell, the right electrode becomes negatively charged. The negative charge on the electrode draws lithium ions in greater number (as seen in Figure 6) and also perturbs their solvation structure, as shown in Figure 9. In the 3V simulations, the non-scaled electrolyte once again shows a consistent EC coordination as lithium approaches the electrode. However, in this case there is also an increase in anion coordination as one approaches the region of higher lithium density before trending downward. The loss of anion coordination in the lithium rich layer is presumably a result of the electrostatic repulsion of the PF₆⁻ from the uniform negative surface charge smeared across the right electrode. The stripping of the counterions has a greater impact on the q-scaled results since the anion makes up a larger contributor to the lithium solvation shell in the bulk solution. The drop in anion coordination from 1.0 to 0.2 is accompanied by an increase in EC coordination that is not seen in the non-scaled simulations.

In summary of our discussion to this point, the contrast between graphite, Li₂EDC, LiF, and Li₂CO₃ suggests that for sufficiently strong ion accumulation, aggregation of ions at the surface tends toward significant aggregation that is less dependent on bulk ion association. This is clearly the case for both LiF and Li₂CO₃. Hence, the relative change for ion-paired electrolytes is less dramatic than for bulk solutions with solvent-separated species. When the ions do not accumulate as strongly at the interface, as in the case of Li₂EDC, the changes in solvation structure are similar regardless of bulk electrolyte structure. With the application of an electric field, the

degree of anion stripping from the lithium is similar, whether the bulk electrolyte is ion pairing or not, but the relative changes are more pronounced if there is strong ion pairing in the bulk electrolyte.

d. Electrolyte Dynamics at the Interface

The final effect of interfaces considered is their impact on electrolyte dynamics at the surface. These changes were quantified by studying the solvation correlation functions for both EC and PF₆, see Eq. (1), around the lithium ion in electrolyte layers as a function of distance from the surface. We have previously shown that the behavior of the solvation correlation function follows that of the surface residence time in quantifying the slowing of the electrolyte at surfaces.⁴⁶ Figure 10 demonstrates the substantial contrast in the residence time as one moves from lithium at the surface to those found in the bulk region. The slower exchange of EC from the lithium solvation shell persists up to a nanometer away from the interface for each SEI considered. The EC solvation correlation function for lithium ions adsorbed to the LiF crystal surface shows a very rigid solvation structure which does not undergo any solvent exchange during the course of the simulation. The lack of solvent exchange evidences the strong binding of the EC to the interface, in agreement with the observations made in our discussion of ion accumulation at this surface. The strong binding of the EC persists even when its charges are scaled, as seen by the lack of solvent exchange when the q-scaled solvent is employed. The strong EC binding at LiF agrees with our assessment that EC-surface binding prevents changes to ion accumulation in swapping the non-scaled and q-scaled electrolytes. Moving away from the LiF surface, the solvation correlation function takes on an intermediate behavior between the bulk and adsorbed layers. The residence times for the EC in this second layer reflect the local increase in ion densities and effective viscosity and thus remain longer than the bulk values. There is a slight increase in how

rapidly the EC correlation decays in the diffuse layer with the q-scaled solvent, which agrees with the weaker binding to the ions that make up the adsorbed layer at the crystal surface. As seen from the study of the bulk electrolyte, once one moves far enough from the surface the difference between the non-scaled and q-scaled electrolytes disappears.

In the case of the Li₂CO₃ surface, we attributed the ion accumulation behavior to a more competitive coordination of the EC and anion to the surface which is also borne out by the behavior of the solvation correlation functions. First, at the surface the function is not flat during the time scale of the simulation, indicating EC solvent exchange occurs, albeit very slowly during the simulation. Second, the use of the q-scaled solvent causes a faster decay, implying that the EC is more free to move in this layer once its charges are reduced and its interaction with the Li₂CO₃ surface is likewise reduced. Moving to the second electrolyte layer, the slight slow down of EC exchange in the q-scaled electrolyte likely arises from the significantly increased amount of ion accumulation at the interface in contrast to the non-scaled result. While the statistics for the correlation functions were slightly worse for Li₂EDC (see Figure S10 in the Supporting Information), it follows the same trends seen for the previous two SEI films. Here the mobility of the EC solvating the lithium ion is greater at the interface, in line with the expectation that the EC binding to the surface is weaker in the case of Li₂EDC than for the other SEI films considered. The impact of reducing the charges on EC is minimal and results in only slightly faster residence times. Finally, in the case of graphite the EC dynamics are not substantially impacted by the charge scaling or the application of bias voltage at the carbon surface (see Figure S11 in the Supporting Information). In summary, the EC solvation dynamics at the film surfaces are significantly slowed by the presence of the inorganic interface and the impact is proportional to the strength of the EC-surface interaction. The effect of the interface on solvent dynamics in the

diffuse region outside the adsorbed layer are fairly muted, but are sensitive to subtle changes in electrolyte structure outside of the adsorbed layer.

Regarding the dynamics of the PF₆⁻ coordination to lithium, the same trends are seen for all of three SEI surfaces and an example is shown for Li₂CO₃ in Figure 11. As seen for EC bound to LiF, the anions at the carbonate crystal are strongly adsorbed to the surface and do not leave the solvation shell of the lithium they are connected to during the time scale of the simulation. Following the adsorbed layer, the anions in the diffuse layer beyond remain coordinated to the lithium ions longer than in the bulk phase, in agreement with the tendency to form larger aggregates at the interface. In comparing the non-scaled and q-scaled results, the anion remains more tightly coordinated in all 3 layers in the q-scaled electrolyte, in agreement with the larger amount of ion association seen in the q-scaled simulations overall. At the graphite surface the behavior of the PF₆⁻ largely follows that seen for the bulk simulations in comparing charge scaled and non-scaled solvents, indicating the relative immunity of the ion dynamics to the graphite surface at 0V (see Figure S11). With the application of a voltage, the PF₆⁻ is more mobile around the lithium ions in agreement with the ion stripping seen in the q-scaled model at 3V.

IV. Conclusions:

The formation and evolution of the SEI in rechargeable batteries is sensitive to the composition and dynamics of the electrolyte layers present at the electrode surface. While experimental techniques for probing this surface remain a challenge, we have compared the expectations for this surface to those of well-studied electrolytes and used extensive classical molecular dynamics simulations to explore the role of several SEI interfaces on altering electrolyte behavior. In order to address general trends, we considered two electrolytes generated by different models of the solvent: partial charges taken directly from DFT calculations and partial charges

scaled by 0.9 to provide better agreement with condensed phase measurements. By comparing the response of the two electrolytes to the interfaces studied herein, we have explored the interplay of solvent-surface attraction and ion association on the accumulation of ions at the SEI, propensity for forming aggregate ion solvation structures, and slowing of solvent exchange. observations suggest that for ionic surfaces, at which there can be strong coordination of the solvent, there is an active competition between solvent molecules and the electrolyte salt that largely impacts the degree of to which excess ions will accumulate. In the q-scaled sovlent, the solvent-surface interaction is weakened which allows for greater ion accumulation and emphasizes the importance of accurate modeling of the solvent–surface interaction. Greater ion accumulation at the inorganic interface drives larger ion association to form aggregate structures with multiple anions coordinating a single lithium. The degree to which this association differs from bulk largely depends on the degree of ion association in the bulk; the transition is more pronounced for weakly associating salts in solution that are driven to form aggregates at the surface than for the electrolyte that already has strong ion association in the bulk. Regarding electrolyte dynamics, both solvent surface interaction and ion association impact the solvent correlation functions. The solventsurface binding plays a significant role in altering the residence time of EC at the surface, while the degree of ion association changes the residence time of the anion across the entire simulation cell. In the context of other modeling efforts at SEI interfaces, our results indicate the potential origins for disagreements arising from different descriptions of surface interactions rather than differences in bulk electrolyte properties. Differences in ion accumulation likely arise from differences in the description of EC-surface binding, while differences seen in ion pairing behavior likely arise from differences in the ion-surface interactions. Hence continued efforts to develop accurate descriptions of electrolyte components at interfaces are vital to the practical application

of classical molecular dynamics simulations to understand the electrolyte/inorganic solid boundary.

V. Supporting Information: Information pertaining to the simulation setup can be found in Table S1 and the structure of Li₂EDC is shown in Figure S1. Additional radial distribution functions describing the bulk electrolyte structure and dynamics are found in Figures S2–S6. Density plots for the EC at the four different interfaces considered are found in Figures S7–S8 and changes in lithium ion coordination as a function of distance from the LiF surface are found in Figure S9. Figure S10–S11 provide plots of the solvation correlation function at Li₂EDC and the graphite electrodes.

VI. Acknowledgements: This work was supported by funding from the Chemical Theory, Modeling, and Computation division of the National Science Foundation (NSF-CHE 1900423). WGD also thanks Villanova University for summer funding in support of this research.

VII. References:

- (1) Chen, S.; Dai, F.; Cai, M. Opportunities and Challenges of High-Energy Lithium Metal Batteries for Electric Vehicle Applications. *ACS Energy Lett.* **2020**, *5* (10), 3140–3151.
- (2) Placke, T.; Kloepsch, R.; Dühnen, S.; Winter, M. Lithium Ion, Lithium Metal, and Alternative Rechargeable Battery Technologies: The Odyssey for High Energy Density. *J. Solid State Electrochem.* **2017**, *21*, 1939–1964.
- (3) Chu, S.; Cui, Y.; Liu, N. The Path towards Sustainable Energy. *Nat. Mater.* **2017**, *16* (1), 16–22.
- (4) Chen, S.; Wen, K.; Fan, J.; Bando, Y.; Goldberg, D. Progress and Future Prospects of High-Voltage and High-Safety Electrolytes in Advanced Lithium Batteries: From Liquid to Solid Electrolytes. *J. Mater. Chem. A* **2018**, *6*, 11631–11663.
- (5) Xu, K. Electrolytes and Interphases in Li-Ion Batteries and Beyond. *Chem. Rev.* 2014, 114(23), 11503–11618.
- (6) Xu, K. Nonaqueous Liquid Electrolytes for Lithium-Based Rechargeable Batteries. Chem. Rev. 2004, 104 (10), 4303–4417.
- (7) Ue, M. Mobility and Ionic Association of Lithium and Quaternary Ammonium Salts in Propylene Carbonate and γ-Butyrolactone. J. Electrochem. Soc. 1994, 141 (12), 3336.
- (8) Klassen, B.; Aroca, R.; Nazri, M.; Nazri, G. a. Raman Spectra and Transport Properties of Lithium Perchlorate in Ethylene Carbonate Based Binary Solvent Systems for Lithium Batteries. *J. Phys. Chem. B* **1998**, *102* (24), 4795–4801.
- (9) Brouillette, D.; Perron, G.; Desnoyers, J. E. Effect of Viscosity and Volume on the

- Specific Conductivity of Lithium Salts in Solvent Mixtures. *Electrochim. Acta* **1999**, *44* (26), 4721–4742.
- (10) Leung, K.; Noked, R.; Noked, M. Anodic Decomposition of Surface Films on High Voltage Spinel Surfaces Density Function Theory and Experimental Study. *J. Chem. Phys.* **2019**, *151* (23), 234713.
- (11) Li, S.; Jiang, M.; Xie, Y.; Xu, H.; Jia, J.; Li, J. Developing High-Performance Lithium Metal Anode in Liquid Electrolytes: Challenges and Progress. *Adv. Mater.* **2018**, *30*, 1706375.
- (12) Li, M.; Wang, C.; Chen, Z.; Xu, K.; Lu, J. New Concepts in Electrolytes. *Chem. Rev.*2020, 120 (14), 6783–6819.
- Gauthier, M.; Carney, T. J.; Grimaud, A.; Giordano, L.; Pour, N.; Chang, H.-H.; Fenning,
 D. P.; Lux, S. F.; Paschos, O.; Bauer, C.; et al. Electrode-Electrolyte Interface in Li-Ion
 Batteries: Current Understanding and New Insights. *J. Phys. Chem. Lett.* 2015, 6 (22),
 4653–4672.
- (14) Markevich, E.; Salitra, G.; Aurbach, D. Fluoroethylene Carbonate as an Important Component for the Formation of an E Ff Ective Solid Electrolyte Interphase on Anodes and Cathodes for Advanced Li-Ion Batteries. *ACS Energy Lett.* **2017**, *2*, 1337–1345.
- (15) Jurng, S.; Brown, Z. L.; Kim, J.; Lucht, B. L. Effect of Electrolyte on the Nanostructure of the Solid Electrolyte Interphase (SEI) and Performance of Lithium Metal Anodes. *Energy Environ. Sci.* **2018**, *11* (9), 2600–2608.
- (16) Takada, K.; Yamada, Y.; Watanabe, E.; Wang, J.; Sodeyama, K.; Tateyama, Y.; Hirata,

- K.; Kawase, T.; Yamada, A. Unusual Passivation Ability of Superconcentrated Electrolytes toward Hard Carbon Negative Electrodes in Sodium-Ion Batteries. *ACS Appl. Mater. Interfaces* **2017**, *9* (39), 33802–33809.
- (17) He, Y.; Fan, W.; Zhang, Y.; Wang, Z.; Li, X.; Liu, Z.; Lü, Z. Understanding the Relationships between Morphology, Solid Electrolyte Interphase Composition, and Coulombic Efficiency of Lithium Metal. ACS Appl. Mater. Interfaces 2020, 12 (19), 22268–22277.
- (18) Heiskanen, S. K.; Kim, J.; Lucht, B. L. Generation and Evolution of the Solid Electrolyte Interphase of Lithium-Ion Batteries. *Joule* **2019**, *3* (10), 2322–2333.
- (19) Winter, M. The Solid Electrolyte Interphase The Most Important and the Least Understood Solid Electrolyte in Rechargeable Li Batteries. *Zeitschrift für Phys. Chemie* 2009, 223 (10–11), 1395–1406.
- (20) Wang, A.; Kadam, S.; Li, H.; Shi, S.; Qi, Y. Review on Modeling of the Anode Solid Electrolyte Interphase (SEI) for Lithium-Ion Batteries. *npj Comput. Mater.* **2018**, *4*, 15.
- (21) Wang, Y.; Sinha, S.; Desai, P. R.; Jing, H.; Das, S. Ion at Air-Water Interface Enhances Capillary Wave Fluctuations: Energetics of Ion Adsorption. J. Am. Chem. Soc. 2018, 140 (40), 12853–12861.
- (22) Dang, L. X.; Schenter, G. K. Rate Theory of Ion Pairing at the Water Liquid-Vapor Interface: A Case of Sodium Iodide. *J. Chem. Phys.* **2018**, *148* (22), 222820.
- (23) Feng, R. R.; Bian, H. T.; Guo, Y.; Wang, H. F. Spectroscopic Evidence for the Specific Na+ and K+ Interactions with the Hydrogen-Bonded Water Molecules at the Electrolyte

- Aqueous Solution Surfaces. J. Chem. Phys. 2009, 130 (13), 134710.
- (24) Cheng, J.; Hoffmann, M. R.; Colussi, A. J. Anion Fractionation and Reactivity at Air/Water:Methanol Interfaces. Implications for the Origin of Hofmeister Effects. *J. Phys. Chem. B* **2008**, *112* (24), 7157–7161.
- Otten, D. E.; Shaffer, P. R.; Geissler, P. L.; Saykally, R. J. Elucidating the Mechanism of Selective Ion Adsorption to the Liquid Water Surface. *Proc. Natl. Acad. Sci. U. S. A.*2012, 109 (3), 701–705.
- (26) Piatkowski, L.; Zhang, Z.; Backus, E. H. G.; Bakker, H. J.; Bonn, M. Extreme Surface Propensity of Halide Ions in Water. *Nat. Commun.* **2014**, *5* (May), 1–7.
- (27) McCaffrey, D. L.; Nguyen, S. C.; Cox, S. J.; Weller, H.; Alivisatos, A. P.; Geissler, P. L.; Saykally, R. J. Mechanism of Ion Adsorption to Aqueous Interfaces: Graphene/Water vs. Air/Water. *Proc. Natl. Acad. Sci. U. S. A.* 2017, 114 (51), 13369–13373.
- (28) Kobayashi, K.; Liang, Y.; Sakka, T.; Matsuoka, T. Molecular Dynamics Study of Salt-Solution Interface: Solubility and Surface Charge of Salt in Water. *J. Chem. Phys.* **2014**, *140* (14), 144705.
- (29) Liu, F.; Sun, D. Ion Distribution and Hydration Structure at Solid-Liquid Interface between NaCl Crystal and Its Solution. *ACS Omega* **2019**, *4* (20), 18692–18698.
- (30) Tuladhar, A.; Piontek, S. M.; Frazer, L.; Borguet, E. Effect of Halide Anions on the Structure and Dynamics of Water next to an Alumina (0001) Surface. *J. Phys. Chem. C* 2018, 122 (24), 12819–12830.
- (31) Yang, Y.; Meng, S. Atomistic Nature of NaCl Nucleation at the Solid-Liquid Interface. J.

- Chem. Phys. 2007, 126 (4), 044708.
- (32) Joung, S.; Cheatham, T. E. Molecular Dynamics Simulations of the Dynamic and Energetic Properties of Alkali and Halide Ions Using Water-Model-Specific Ion Parameters. *J. Phys. Chem. B* **2009**, *113* (40), 13279–13290.
- (33) Wang, R.; Dellostritto, M.; Remsing, R. C.; Carnevale, V.; Klein, M. L.; Borguet, E. Sodium Halide Adsorption and Water Structure at the α-Alumina(0001)/Water Interface.
 J. Phys. Chem. C 2019, 123, 15618–15628.
- (34) Vazdar, M.; Pluhařová, E.; Mason, P. E.; Vácha, R.; Jungwirth, P. Ions at Hydrophobic Aqueous Interfaces: Molecular Dynamics with Effective Polarization. *J. Phys. Chem. Lett.* **2012**, *3* (15), 2087–2091.
- (35) Kumar, N.; Servis, M. J.; Liu, Z.; Clark, A. E. Competitive Interactions at Electrolyte/Octanol Interfaces: A Molecular Perspective. J. Phys. Chem. C 2020, 124 (20), 10924–10934.
- (36) Andersson, G.; Ridings, C. Ion Scattering Studies of Molecular Structure at Liquid Surfaces with Applications in Industrial and Biological Systems. *Chem. Rev.* 2014, 114 (17), 8361–8387.
- (37) Jungwirth, P.; Winter, B. Ions at Aqueous Interfaces: From Water Surface to Hydrated Proteins. *Annu. Rev. Phys. Chem.* **2008**, *59* (1), 343–366.
- Jungwirth, P.; Tobias, D. J. Specific Ion Effects at the Air/Water Interface. *Chem. Rev.*2006, 106 (4), 1259–1281.
- (39) Venkateshwaran, V.; Vembanur, S.; Garde, S. Water-Mediated Ion-Ion Interactions Are

- Enhanced at the Water Vapor-Liquid Interface. *Proc. Natl. Acad. Sci. U. S. A.* **2014**, *111* (24), 8729–8734.
- (40) Smith, J. D.; Rick, S. W. Ion Clustering in Aqueous Salt Solutions near the Liquid/Vapor Interface. *Condens. Matter Phys.* **2016**, *19* (2), 1–10.
- (41) Le Crom, S.; Tournassat, C.; Robinet, J.-C.; Marry, V. Influence of Polarizability on the Prediction of the Electrical Double Layer Structure in a Clay Mesopore: A Molecular Dynamics Study. *J. Phys. Chem. C* **2020**, *124* (11), 6221–6232.
- (42) Kiyohara, K.; Minami, R. Hydration and Dehydration of Monovalent Cations near an Electrode Surface Hydration and Dehydration of Monovalent Cations near an Electrode Surface. *J. Chem. Phys.* **2018**, *149* (1), 014705.
- Zhan, C.; Cerón, M. R.; Hawks, S. A.; Otani, M.; Wood, B. C.; Pham, T. A.; Stadermann,
 M.; Campbell, P. G. Specific Ion Effects at Graphitic Interfaces. *Nat. Commun.* 2019, *10*(1), 1–8.
- (44) Vila Verde, A.; Lipowsky, R. Cooperative Slowdown of Water Rotation near Densely Charged Ions Is Intense but Short-Ranged. *J. Phys. Chem. B* **2013**, *117* (36), 10556–10566.
- (45) Nguyen, M.; Rick, S. W. The Influence of Polarizability and Charge Transfer on Specific Ion Effects in the Dynamics of Aqueous Salt Solutions. *J. Chem. Phys.* **2018**, *148* (22).
- (46) Raguette, L.; Jorn, R. Ion Solvation and Dynamics at Solid Electrolyte Interphases: A Long Way from Bulk? *J. Phys. Chem. C* **2018**, *122* (6), 3219–3232.
- (47) Jorn, R.; Raguette, L.; Peart, S. Investigating the Mechanism of Lithium Transport at

- Solid Electrolyte Interphases. J. Phys. Chem. C 2020, 124 (30), 16261–16270.
- (48) Oh, M. I.; Gupta, M.; Weaver, D. F. Understanding Water Structure in an Ion-Pair Solvation Shell in the Vicinity of a Water/Membrane Interface. *J. Phys. Chem. B* **2019**, *123* (18), 3945–3954.
- (49) Borodin, O.; Zhuang, G. V.; Ross, P. N.; Xu, K. Molecular Dynamics Simulations and Experimental Study of Lithium Ion Transport in Dilithium Ethylene Dicarbonate. *J. Phys. Chem. C* **2013**, *117* (15), 7433–7444.
- (50) Warren, G. L.; Patel, S. Electrostatic Properties of Aqueous Salt Solution Interfaces: A Comparison of Polarizable and Nonpolarizable Ion Models. J. Phys. Chem. B 2008, 112 (37), 11679–11693.
- (51) Zhang, B.; Lin, Z.; Chen, H.; Wang, L. W.; Pan, F. The Stability and Reaction Mechanism of a LiF/Electrolyte Interface: Insight from Density Functional Theory. *J. Mater. Chem. A* **2020**, *8* (5), 2613–2617.
- (52) Borodin, O.; Bedrov, D. Interfacial Structure and Dynamics of the Lithium Alkyl Dicarbonate SEI Components in Contact with the Lithium Battery Electrolyte. *J. Phys. Chem. C* **2014**, *118* (32), 18362–18371.
- (53) Jorn, R.; Kumar, R.; Abraham, D. P.; Voth, G. A. Atomistic Modeling of the Electrode–Electrolyte Interface in Li-Ion Energy Storage Systems: Electrolyte Structuring. *J. Phys. Chem. C* **2013**, *117* (8), 3747–3761.
- (54) Vatamanu, J.; Borodin, O.; Smith, G. D. Molecular Dynamics Simulation Studies of the Structure of a Mixed Carbonate/LiPF6 Electrolyte near Graphite Surface as a Function of

- Electrode Potential. J. Phys. Chem. C 2011, 116, 1114–1121.
- (55) Smith, G. D.; Borodin, O.; Russo, S. P.; Rees, R. J.; Hollenkamp, A. F. A Molecular Dynamics Simulation Study of LiFePO4/Electrolyte Interfaces: Structure and Li+ Transport in Carbonate and Ionic Liquid Electrolytes. *Phys. Chem. Chem. Phys.* 2009, 11, 9884–9897.
- (56) Raberg, J. H.; Vatamanu, J.; Harris, S. J.; Van Oversteeg, C. H. M.; Ramos, A.; Borodin,
 O.; Cuk, T. Probing Electric Double-Layer Composition via in Situ Vibrational
 Spectroscopy and Molecular Simulations. *J. Phys. Chem. Lett.* 2019, 10 (12), 3381–3389.
- (57) Duboué-Dijon, E.; Javanainen, M.; Delcroix, P.; Jungwirth, P.; Martinez-Seara, H. A Practical Guide to Biologically Relevant Molecular Simulations with Charge Scaling for Electronic Polarization. J. Chem. Phys. 2020, 153 (5), 050901.
- (58) Leontyev, I.; Stuchebrukhov, A. Accounting for Electronic Polarization in Non-Polarizable Force Fields. *Phys. Chem. Chem. Phys.* **2011**, *13* (7), 2613–2626.
- (59) Kirby, B. J.; Jungwirth, P. Charge Scaling Manifesto: A Way of Reconciling the Inherently Macroscopic and Microscopic Natures of Molecular Simulations. *J. Phys. Chem. Lett.* 2019, 10 (23), 7531–7536.
- (60) Chaudhari, M. I.; Nair, J. R.; Pratt, L. R.; Soto, F. A.; Balbuena, P. B.; Rempe, S. B. Scaling Atomic Partial Charges of Carbonate Solvents for Lithium Ion Solvation and Diffusion. J. Chem. Theory Comput. 2016, 12, 5709–5718.
- (61) Arslanargin, A.; Powers, A.; Beck, T. L.; Rick, S. W. Models of Ion Solvation

 Thermodynamics in Ethylene Carbonate and Propylene Carbonate. *J. Phys. Chem. B*

- **2016**, *120*, 1497–1508.
- (62) Bedrov, D.; Piquemal, J. P.; Borodin, O.; MacKerell, A. D.; Roux, B.; Schröder, C. Molecular Dynamics Simulations of Ionic Liquids and Electrolytes Using Polarizable Force Fields. *Chem. Rev.* 2019, 119 (13), 7940–7995.
- (63) Sun, H.; Mumby, S. J.; Maple, J. R.; Hagler, A. T. An Ab Initio CFF93 All-Atom Force Field for Polycarbonates. *J. Am. Chem. Soc.* **1994**, *116* (7), 2978–2987.
- (64) Tasaki, K. Solvent Decompositions and Physical Properties of Decomposition Compounds in Li-Ion Battery Electrolytes Studied by DFT Calculations and Molecular Dynamics Simulations. J. Phys. Chem. B 2005, 109 (7), 2920–2933.
- (65) Tasaki, K.; Harris, S. J. Computational Study on the Solubility of Lithium Salts Formed on Lithium Ion Battery Negative Electrode in Organic Solvents. *J. Phys. Chem. C* **2010**, *114* (17), 8076–8083.
- (66) Masia, M.; Probst, M.; Rey, R. Ethylene Carbonate-Li+: A Theoretical Study of Structural and Vibrational Properties in Gas and Liquid Phases. *J. Phys. Chem. B* **2004**, *108*, 2016–2027.
- (67) Plimpton, S. Fast Parallel Algorithms for Short-Range Molecular Dynamics. *J. Comput. Phys.* **1995**, *117* (1), 1–19.
- (68) https://lammps.sandia.gov/.
- (69) Golze, D.; Hutter, J.; Iannuzzi, M. Wetting of Water on Hexagonal Boron Nitride@Rh(111): A QM/MM Model Based on Atomic Charges Derived for Nano-Structured Substrates. *Phys. Chem. Chem. Phys.* **2015**, *17* (22), 14307–14316.

- (70) Kühne, T. D.; Iannuzzi, M.; Del Ben, M.; Rybkin, V. V.; Seewald, P.; Stein, F.; Laino, T.; Khaliullin, R. Z.; Schütt, O.; Schiffmann, F.; et al. CP2K: An Electronic Structure and Molecular Dynamics Software Package -Quickstep: Efficient and Accurate Electronic Structure Calculations. *J. Chem. Phys.* 2020, 152 (19), 194103.
- (71) https://www.cp2k.org/.
- (72) Chaudhari, M. I.; Muralidharan, A.; Pratt, L. R.; Rempe, S. B. Assessment of Simple Models for Molecular Simulation of Ethylene Carbonate and Propylene Carbonate as Solvents for Electrolyte Solutions. *Top. Curr. Chem.* **2018**, *376*, 7.
- (73) Thenuwara, A. C.; Shetty, P. P.; McDowell, M. T. Distinct Nanoscale Interphases and Morphology of Lithium Metal Electrodes Operating at Low Temperatures. *Nano Lett.* 2019, 19 (12), 8664–8672.
- Huang, W.; Attia, P. M.; Wang, H.; Renfrew, S. E.; Jin, N.; Das, S.; Zhang, Z.; Boyle, D.
 T.; Li, Y.; Bazant, M. Z.; et al. Evolution of the Solid-Electrolyte Interphase on
 Carbonaceous Anodes Visualized by Atomic-Resolution Cryogenic Electron Microscopy.
 Nano Lett. 2019, 19 (8), 5140–5148.
- (75) Huang, W.; Boyle, D. T.; Li, Y.; Li, Y.; Pei, A.; Chen, H.; Cui, Y. Nanostructural and Electrochemical Evolution of the Solid-Electrolyte Interphase on CuO Nanowires Revealed by Cryogenic-Electron Microscopy and Impedance Spectroscopy. *ACS Nano* **2019**, *13* (1), 737–744.
- (76) Zhang, Q.; Pan, J.; Lu, P.; Liu, Z.; Verbrugge, M. W.; Sheldon, B. W.; Cheng, Y. T.; Qi, Y.; Xiao, X. Synergetic Effects of Inorganic Components in Solid Electrolyte Interphase on High Cycle Efficiency of Lithium Ion Batteries. *Nano Lett.* 2016, *16* (3), 2011–2016.

- (77) Martínez, L.; Andrade, R.; Birgin, E. G.; Martínez, J. M. Packmol: A Package for Building Initial Configurations for Molecular Dynamics Simulations. *J. Comput. Chem.* 2009, 30, 2157–2164.
- (78) Petersen, M. K.; Kumar, R.; White, H. S.; Voth, G. A. A Computationally Efficient Treatment of Polarizable Electrochemical Cells Held at a Constant Potential. *J. Phys. Chem. C* **2012**, *116* (7), 4903–4912.
- (79) Ong, M. T.; Verners, O.; Draeger, E. W.; van Duin, A. C. T.; Lordi, V.; Pask, J. E. Lithium Ion Solvation and Diffusion in Bulk Organic Electrolytes from First-Principles and Classical Reactive Molecular Dynamics. *J. Phys. Chem. B* **2015**, *119* (4), 1535–1545.
- (80) Borodin, O.; Olguin, M.; Ganesh, P.; Kent, P. R. C.; Allen, J. L.; Henderson, W. A. Competitive Lithium Solvation of Linear and Cyclic Carbonates from Quantum Chemistry. *Phys. Chem. Chem. Phys.* **2016**, *18* (1), 164–175.
- (81) Allen, J. L.; Borodin, O.; Seo, D. M.; Henderson, W. A. Combined Quantum Chemical/Raman Spectroscopic Analyses of Li+ Cation Solvation: Cyclic Carbonate Solvents - Ethylene Carbonate and Propylene Carbonate. *J. Power Sources* 2014, 267, 821–830.
- (82) Bogle, X.; Vazquez, R.; Greenbaum, S.; Cresce, A. V. W.; Xu, K. Understanding Li+-Solvent Interaction in Nonaqueous Carbonate Electrolytes with 170 NMR. *J. Phys. Chem. Lett.* **2013**, *4* (10), 1664–1668.
- (83) Peng, J.; Gobet, M.; Devany, M.; Xu, K.; Cresce, A. von W.; Borodin, O.; Greenbaum, S. Multinuclear Magnetic Resonance Investigation of Cation-Anion and Anion-Solvent Interactions in Carbonate Electrolytes. *J. Power Sources* 2018, 399, 215–222.

- (84) Ravikumar, B.; Mynam, M.; Rai, B. Effect of Salt Concentration on Properties of Lithium Ion Battery Electrolytes: A Molecular Dynamics Study. *J. Phys. Chem. C* **2018**, *122* (15), 8173–8181.
- (85) Seo, D. M.; Reininger, S.; Kutcher, M.; Redmond, K.; Euler, W. B.; Lucht, B. L. Role of Mixed Solvation and Ion Pairing in the Solution Structure of Lithium Ion Battery Electrolytes. J. Phys. Chem. C 2015, 119 (25), 14038–14046.
- (86) Fulfer, K. D.; Kuroda, D. G. Solvation Structure and Dynamics of the Lithium Ion in Organic Carbonate-Based Electrolytes: A Time-Dependent Infrared Spectroscopy Study. *J. Phys. Chem. C* 2016, 120 (42), 24011–24022.
- (87) Borodin, O.; Smith, G. D. Quantum Chemistry and Molecular Dynamics Simulation Study of Dimethyl Carbonate: Ethylene Carbonate Electrolytes Doped with LiPF₆. *J. Phys. Chem. B* **2009**, *113* (6), 1763–1776.
- (88) Von Wald Cresce, A.; Gobet, M.; Borodin, O.; Peng, J.; Russell, S. M.; Wikner, E.; Fu, A.; Hu, L.; Lee, H. S.; Zhang, Z.; et al. Anion Solvation in Carbonate-Based Electrolytes. *J. Phys. Chem. C* 2015, *119* (49), 27255–27264.
- (89) Hayamizu, K. Temperature Dependence of Self-Di Ffusion Coefficients of Ions and Solvents in Ethylene Carbonate, Propylene Carbonate, and Diethyl Carbonate Single Solutions and Ethylene Carbonate + Diethyl Carbonate Binary Solutions of LiPF6 Studied by NMR. J. Chem. Eng. Data 2012, 57, 2012–2017.
- (90) Lu, D.; Tao, J.; Yan, P.; Henderson, W. A.; Li, Q.; Shao, Y.; Helm, M. L.; Borodin, O.; Gra, G. L.; Polzin, B.; et al. Formation of Reversible Solid Electrolyte Interface on Graphite Surface from Concentrated Electrolytes. *Nano Lett.* 2017, 17 (3), 1602–1609.

- (91) von Wald Cresce, A.; Borodin, O.; Xu, K. Correlating Li + Solvation Sheath Structure with Interphasial Chemistry on Graphite. *J. Phys. Chem. C* **2012**, *116* (50), 26111–26117.
- (92) Nie, M.; Abraham, D. P.; Seo, D. M.; Chen, Y.; Bose, A.; Lucht, B. L. Role of Solution Structure in Solid Electrolyte Interphase Formation on Graphite with LiPF6 in Propylene Carbonate. *J. Phys. Chem. C* **2013**, *117* (48), 25381–25389.
- (93) Zhang, X. Q.; Chen, X.; Hou, L. P.; Li, B. Q.; Cheng, X. B.; Huang, J. Q.; Zhang, Q. Regulating Anions in the Solvation Sheath of Lithium Ions for Stable Lithium Metal Batteries. *ACS Energy Lett.* **2019**, *4* (2), 411–416.

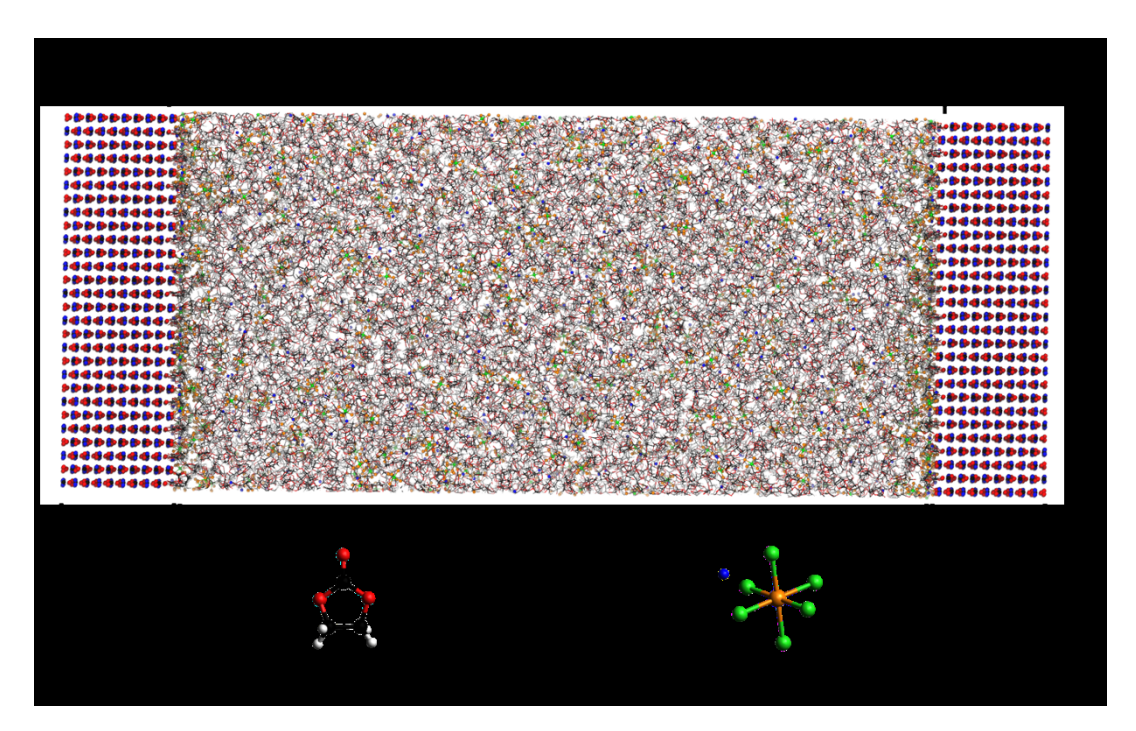


Figure 1. Snapshot of the Li_2CO_3 SEI films interfaced with an electrolyte region consisting of ethylene carbonate (EC) mixed with LiPF₆ (molecular structures shown in the inset). Atoms are color-coded for carbon (black), oxygen (red), hydrogen (white), phosphorous (orange), fluorine (green), and lithium (blue). A location in the electrolyte with respect to the surface of the SEI film is denoted as \boldsymbol{Z} throughout the text for each of the SEI considered and reported quantities are averaged over both electrolyte/SEI surfaces present.

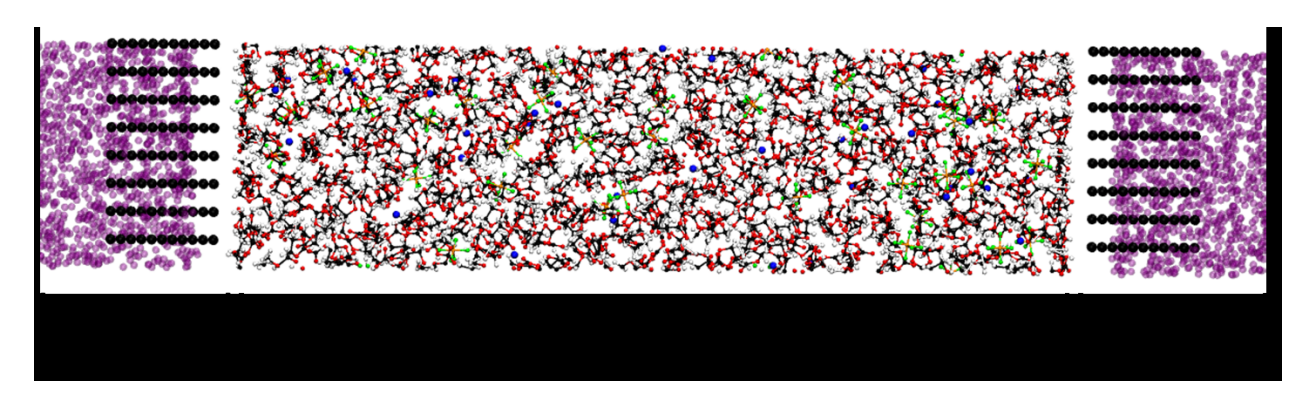


Figure 2. A snapshot of the graphite electrode is shown interfaced with an electrolyte region consisting of ethylene carbonate (EC) and LiPF₆ (see Figure 1 for structures and color coding). Image charges are indicated by purple spheres and the sign of the surface charges with the application of a voltage are indicated in parentheses next to the electrode labels.

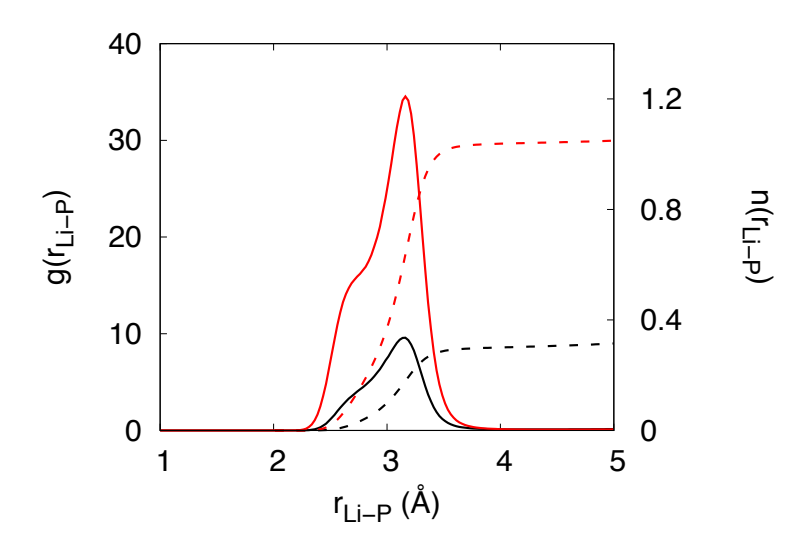


Figure 3. The radial distribution functions (solid lines) are shown for the lithium—phosphorous pair in the bulk electrolyte at 453K described by the non-scaled (black) and q-scaled (red) force fields. The coordination number for phosphorous around the lithium ion are also shown for both models (dashed lines).

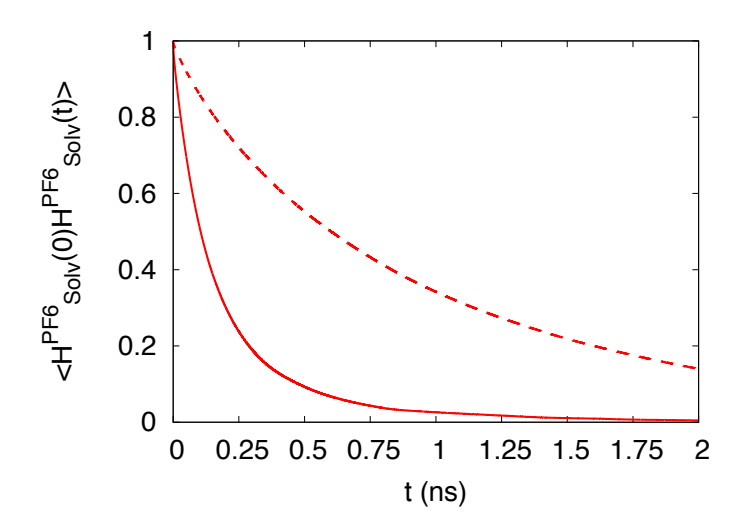


Figure 4. The solvation residence correlation function is shown for PF₆⁻ coordinated to Li⁺ in both the non-scaled (solid) and q-scaled (dashed) models at 453K. The lines were fitted to a stretched exponential of the form $e^{-\left(\frac{t}{\tau}\right)^{\alpha}}$ to extract the average residence lifetime τ .

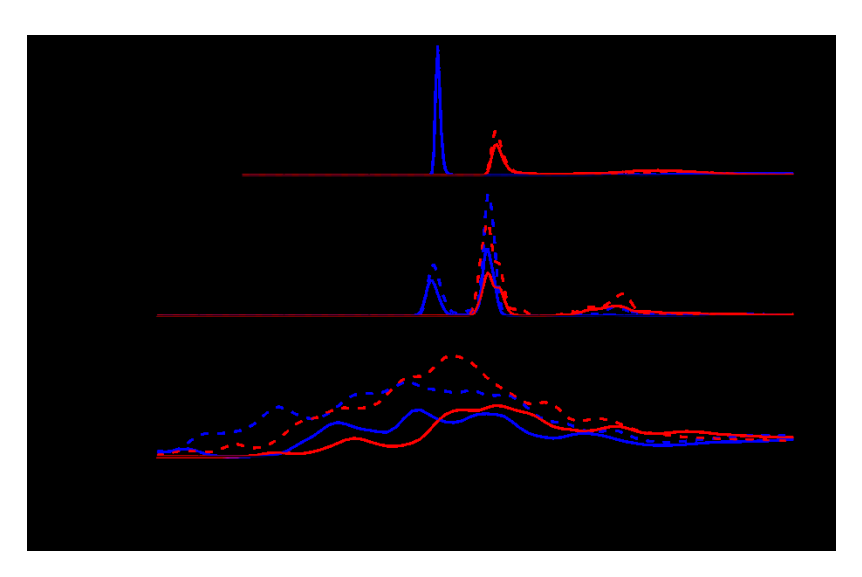


Figure 5. Plots of the lithium (blue) and PF₆ (red) center-of-mass density at the SEI interfaces using the non-scaled (solid) and q-scaled (dashed) force fields. Results are shown at the (a) LiF [100], (b) Li₂CO₃ [010], and (c) amorphous Li₂EDC surfaces and the origin is set to the location of the surface film. Each curve has been normalized by dividing the density by its average value in the middle of the cell.

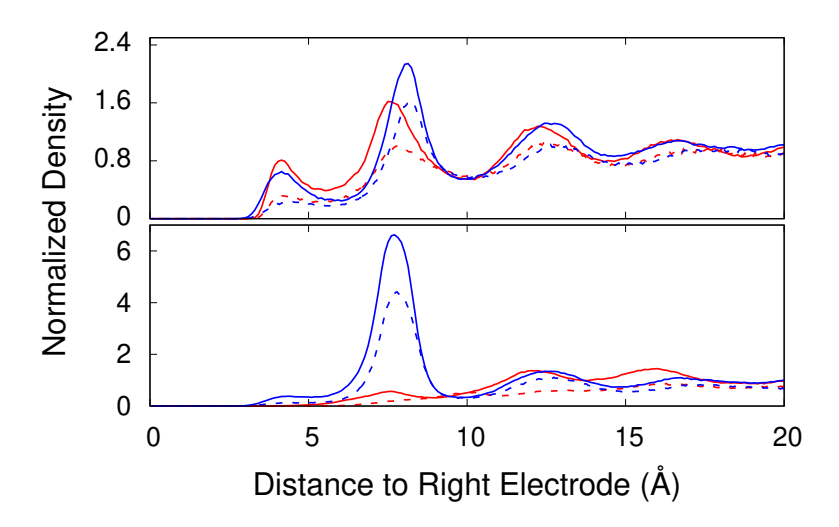


Figure 6. Plots of the lithium (blue) and PF₆–(red) center-of-mass density at the graphite edge plane surface of the right electrode at 0V (top panel) and at a total potential drop of 3V (bottom panel) across the simulation cell. Each curve has been normalized by dividing by the respective ion density in the middle of each simulation cell. Results are shown for the non-scaled model (solid) and q-scaled model (dashed).

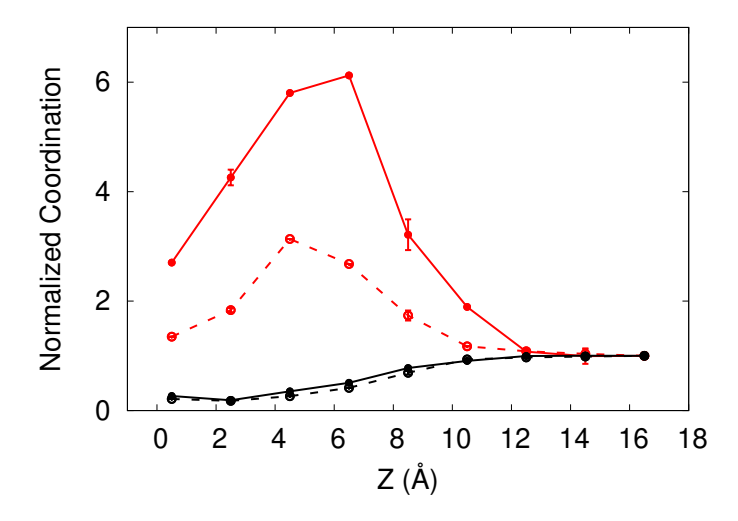


Figure 7. Coordination of lithium ions by the PF_6^- phosphorous (red) and EC carbonyl oxygen (black) as a function of distance from the Li_2CO_3 surface. All curves are normalized to their bulk values and the results from the non-scaled (solid) and q-scaled (dashed) force fields are compared. Error bars are shown for representative points from block averaging across the production trajectories.

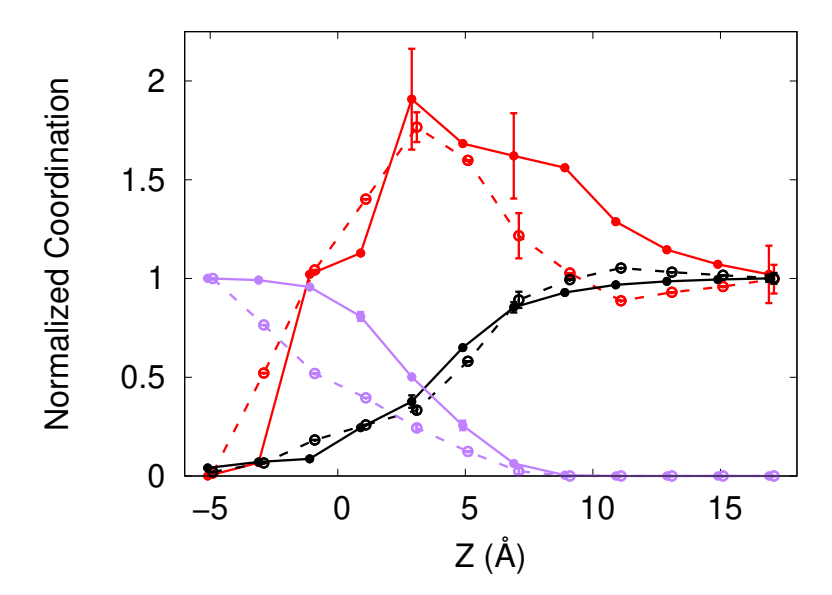


Figure 8. Coordination of lithium ions by the PF₆⁻ phosphorous(red), EC carbonyl oxygen (black), and Li₂EDC carbonate oxygens (purple) as a function of distance from the Li₂EDC surface. All curves are normalized to their bulk values and the results from the non-scaled (solid) and q-scaled (dashed) force fields are compared. Error bars are shown for representative points from block averaging across the production trajectories.

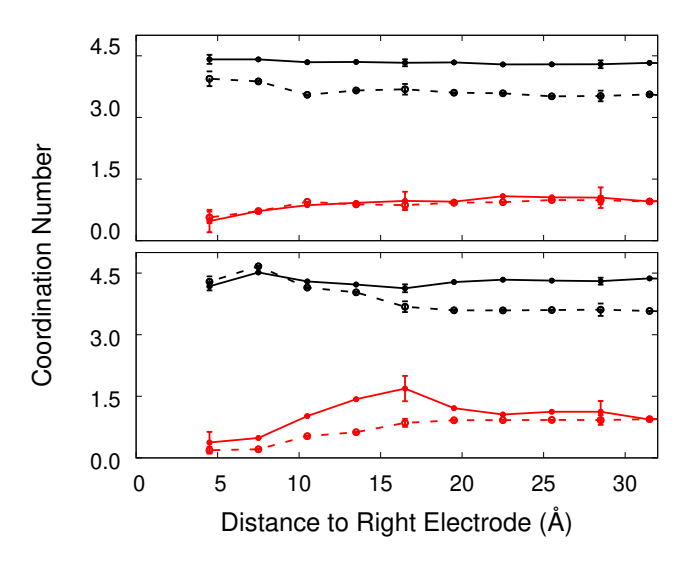


Figure 9. Coordination of lithium ions by the PF₆⁻ phosphorous(red), EC carbonyl oxygen (black), as a function of distance from the graphite electrode surface. The results for phosphorous coordination have been scaled by their bulk values for graphing purposes. Curves are shown for both the non-scaled (solid) and q-scaled (dashed) force fields under 0V(upper panel) and 3V(lower panel) conditions. Error bars are shown for representative points from block averaging across the production trajectories.

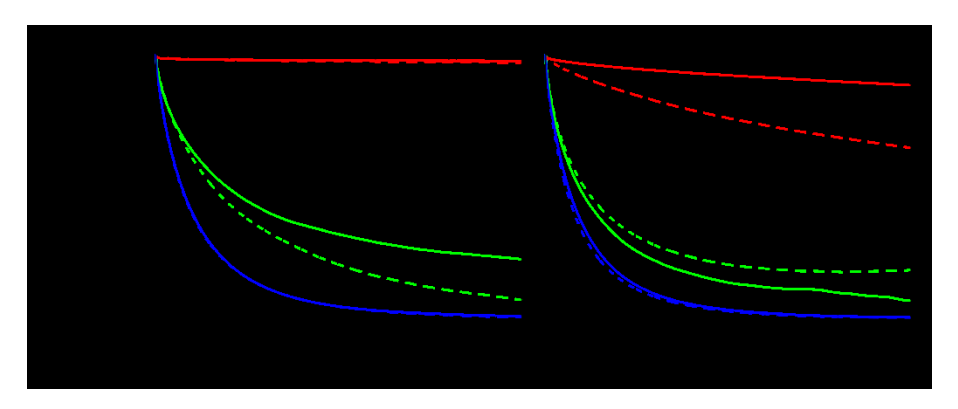


Figure 10. The solvation correlation function for EC coordinating lithium ions, see Eq. (1), is shown in 5–7Å layers centered around 3 Å from the surface (red), 9 Å from the surface (green), and the middle of the simulation cell (blue). Results are shown at the LiF surface (left panel) and Li₂CO₃ surface (right panel) using the non-scaled (solid) and q-scaled (dashed) models.

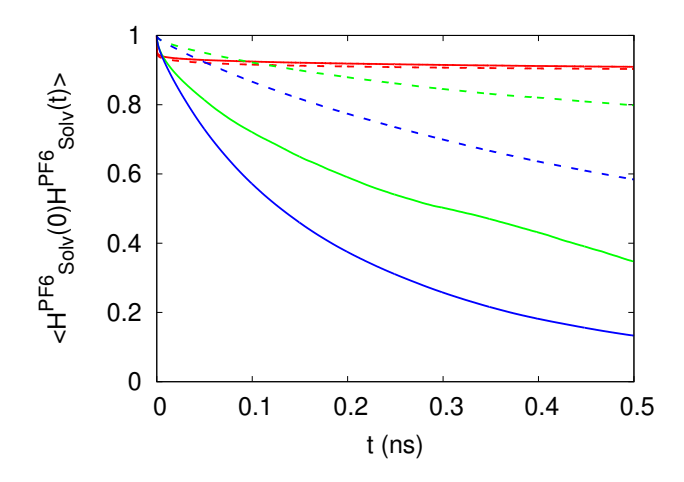
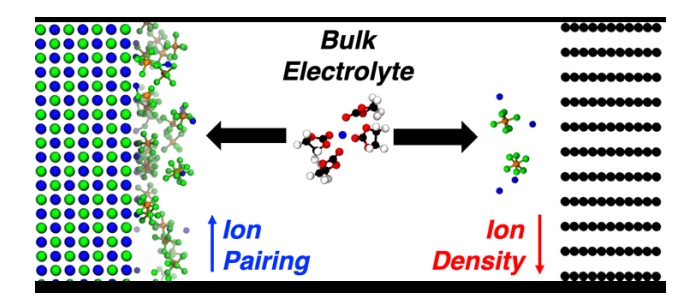


Figure 11. The solvation correlation function for PF₆⁻ coordinating lithium ions is shown for 5–7Å layers centered around 3 Å (red), 9 Å (green), and the middle of the simulation cell (blue) from the Li₂CO₃ surface. Results are shown using the non-scaled (solid) and q-scaled (dashed) models.



TOC Figure.